RESEARCH



Thermal and flow analysis of chemically reactive Casson hybrid nanofluids with machine learning validation

P. Priyadharshini¹ · M. Sowndharya¹ · Ali J. Chamkha²

Received: 5 May 2025 / Accepted: 3 August 2025 / Published online: 20 August 2025 © The Author(s), under exclusive licence to Springer Nature B.V. 2025

Abstract

Background: This research investigates the magnetohydrodynamic flow of a chemically reactive Casson hybrid nanofluid within a Sodium Alginate base, flowing over a curved stretching surface in a porous environment. The analysis accounts for internal heat sources, magnetic field influence, reactive diffusion, and thermophoretic effects to improve thermal performance. Methodology: The model considers transport effects, including Brownian motion, thermophoresis, internal heating, viscosity, and Arrhenius-type reactions. Similarity transformations reduce the governing PDEs to ODEs, which are solved using MATLAB's BVP4c. The sensitivity of thermal and flow parameters is further evaluated using Multiple Linear Regression (MLR). Core findings: Results indicate that elevating the Biot number can boost the Nusselt number by approximately 42%, emphasizing improved heat transfer at the surface. The heat generation parameter exerts the strongest effect on thermal output, with a sensitivity index peaking at 2.8673. Furthermore, the curvature parameter plays a significant role in modulating surface shear. The sensitivity analysis pinpoints parameter combinations that yield optimal performance, reinforcing the utility of machine learning in fluid system optimization. Validation: Comparisons to previous studies demonstrate excellent agreement, as deviations remain under 1.6% for skin friction and 2.3% for the Nusselt number when the curvature parameter equals zero. These results affirm the robustness of the applied transformations and numerical approach. Furthermore, the MLR model perfectly matches numerical outputs, reaching an R^2 score of 1.0, confirming predictive accuracy. **Applications:** The findings reference engineering applications, specifically solar thermal systems, HVAC equipment, and miniaturized heat exchangers. By combining numerical modeling with machine learning, this study offers a reliable approach for designing and controlling energy-efficient thermal systems under varying physical conditions.

P. Priyadharshini

priyadharshinip@psgcas.ac.in

M. Sowndharya sowndharya22897@gmail.com

A.J. Chamkha a.chamkha@kcst.edu.kw

- Department of Mathematics, PSG College of Arts & Science, Coimbatore, Tamil Nadu 641 014, India
- Department of Mechanical Engineering, Kuwait College of Science and Technology, Doha District, 35004, Kuwait



 $\textbf{Keywords} \ \ Casson \ hybrid \ nanofluid \cdot Curved \ surface \cdot Multiple \ linear \ regression \cdot Sensitivity \ analysis$

Abbreviations

- a aspect ratio
- U, V velocity components along x and y axes
- B_0 Magnetic field
- C Fluid Concentration
- R Geometrical radius
- c_p Specific heat capacity at constant temperature
- Biot number
- h_f Coefficient of heat transfer
- K_r Chemical reaction coefficient
- E_a Activation energy coefficient
- P Pressure
- k Curvature factor
- D_{R} Brownian diffusion coefficient
- δ_T Temperature difference factor
- *Nb* Brownian motion parameter
- D_T Thermophoretic diffusion coefficient
- Pr Prandtl number
- Sc Schmidt number
- M Magnetic field parameter
- Ec Eckert number
- r. s Cartesian coordinates
- K Thermal conductivity
- E Activation energy factor
- Q Heat source parameter
- *Nt* Thermophoresis parameter
- T Fluid Temperature
- U_w Velocity of the stretching sheet
- β Casson fluid parameter
- η Similarity independent variable
- μ Fluid viscosity
- v_f Kinematic viscosity
- Φ Volume fraction
- ρ Fluid density
- σ Electrical conductivity
- τ Relative heat capacity (nanoparticle/fluid)
- θ Dimensionless temperature
- Ω Chemical reaction parameter
- ∞ Ambient condition
- w Conditions at the wall

1 Introduction

Casson hybrid nanofluids are a family of fluids with non-Newtonian rheology that combine the shear-thinning characteristics of Casson fluids with the enhanced thermal properties of



hybrid nanofluids—fluids containing more than one type of nanoparticle suspended in a base liquid. The Casson model accurately characterizes yield-stress fluids such as blood, paints, and specific polymers that remain solid until the applied stress surpasses a defined threshold.

Recent advancements have highlighted the strategic integration of hybrid nanoparticles into Casson fluids, owing to their augmented thermal conductivity, superior energy transport efficiency, and tunable non-Newtonian rheological properties, making them highly suitable for complex thermal system applications. These boosted fluids benefit advanced engineering applications, including cooling systems, biomedical treatments, energy storage devices, and manufacturing processes where precise thermal control is critical. Raptis et al. (2004) flow exhibiting asymmetry, wherein an electrically conducting fluid interacts with a semiinfinite stationary boundary under radiative heat transfer effects. Sodium Alginate is utilized as the carrier fluid, serving as a representative example of a Casson-type Complex fluid. Khan et al. (2018) integrated radiative transfer effects, internal heat generation, magnetic fields, and porous media to simulate realistic physical phenomena. Aladdin et al. (2020) assessed the effect of wall suction and heat transfer across a moving boundary. Nadeem et al. (2023) observed that Casson effects and surface thickness reduce velocity across all models, providing insights into nanofluid flow regulation. Farooq et al. (2024) determine that the heat dissipation rate consistently improves across all examined parameters, with documented convergence ranges, highlighting the effectiveness of Advancements in thermal control through hybrid nanofluids for nanotechnology applications. Hybrid nanofluids formulated with Sodium Alginate (SA) offer enhanced heat transfer capabilities, exhibiting superior thermal and physical properties compared to conventional base fluids. Due to their improved thermal conductivity, these hybrid nanofluids are increasingly recognized for their potential in high-performance thermal systems. Hussanan et al. (2020) explore the thermal performance improvement of a viscoplastic non-Newtonian hybrid nanofluid formulated by suspending Copper (Cu) and Magnetite $(Fe_3 O_4)$ nanoparticles within an SAbase fluid. The combined presence of non-magnetic and magnetic nanoparticles in a non-Newtonian matrix offers a unique avenue for optimizing thermal performance in complex flow environments. Focusing on viscous dissipation effects, Rehman et al. (2024) analyze a Casson hybrid nanofluid's time-dependent magnetohydrodynamic (MHD) flow characteristics, incorporating a couple of stress influences over a deformable stretching surface. Shah et al. (2024) scrutinize that increasing copper content augments heat transfer while stronger magnetic fields reduce thermal boundary layer thickness. Stability analysis confirms the physically realizable solution under selected parameter ranges. Razaq et al. (2023) observe that entropy generation increases significantly under the influence of strong radiative heat flux and diffusion, indicating greater irreversibility in the system. Their findings also showed that thermal transport improves with higher radiation parameters and extended thermal relaxation time, emphasizing their importance in enhancing energy transfer efficiency in nanofluid flows. Similarly, Hayat et al. (2024) examine hydromagnetic mixed convection in Reiner–Rivlin fluids with variable thermophysical properties, demonstrating its relevance to advanced thermal and chemical engineering applications. Additionally, Yusuf et al. (2023, 2024), Yusuf (2024) explore MHD nanofluid flow over a stretching sheet, considering variable viscosity and non-uniform heat generation effects. Sajjan et al. (2023) investigate the slender surface flow characteristics in the presence of ternary nanoparticles using MATLAB bvp5c solver. Akbar et al. (2023) reveal that Casson hybrid nanofluids display contrasting flow characteristics between stretching and shrinking channel walls. For stretching surfaces, augmenting the Casson parameter intensifies shear stress and heat transfer in the stretching scenario, reducing these effects under shrinking conditions. Fluid flow over stationary and moving surfaces is crucial in numerous industrial applications, including metal forming, film



extrusion, and fiber cooling. In light of these applications, Shankaralingappa et al. (2021) investigate the volumetric, incompressible, laminar flow of a Casson nanofluid affected by thermophoretic particle deposition across a nonlinearly stretching surface. Abo-Dahab et al. (2021) propose an integrated approach to modeling Casson nanofluid dynamics under multiple physical influences, including nanoparticle diffusion and reactive mass transport. Abbas et al. (2013) expose that multiplying the radius of curvature and Hartmann number significantly alters the flow velocity and thermal distributions. Moreover, higher magnetic field strength amplifies flow resistance while reducing the heat transfer rate, as reflected in the profile of shear stress and thermal transport. Ahmad et al. (2019) by employing curvilinear coordinates to capture the geometry's curvature and solving the reduced equations using MATLAB's bvp4c, this work provides a comparative assessment against flat surface results, offering fresh perspectives on flow dynamics in curved porous domains. The results show that higher magnetic and porosity parameters increase skin friction, consistent with earlier research. Following the observation, Dawar et al. (2023a) highlight the effectiveness of Casson-based hybrid nanofluids in Boosting thermal performance and fluid dynamics within engineering systems, particularly in MHD and non-Newtonian fluid systems. Jamshed et al. (2021) examine unsteady heat transport and entropy generation in Solar-heated convective flow of a Casson nanofluid across a surface with slip conditions. Results show enhanced thermal conductivity, with copper-water nanofluid offering superior heat transfer. Irfan et al. (2017) assess the unsteady 3D flow of a Carreau nanofluid on a bi-directionally stretching sheet, accounting for spatially varying thermal conductivity and the presence of internal heat sources. A modified zero mass flux condition improves nanoparticle behavior modeling within Buongiorno's framework. Lund et al. (2023) inspect the thermal behavior of a magnetized Casson-based hybrid nanofluid, formulated with Sodium Alginate and infused with Aluminum Oxide and Copper nanoparticles, flowing over a permeable, moving surface. The analysis incorporates the impact of electrical heating and thermal radiation, modeled using the Tiwari-Das approach. Raza et al. (2024) focus on the thermal characteristics of Casson nanofluid motion along an extending surface, incorporating the consequence of activation energy, magnetic field influence, and velocity slip to enhance the model's physical accuracy.

The study analyzes heat transfer characteristics of Cu-Al₂O₃/SA nanofluids exposed to solar radiation, aiming to boost the performance of flat-plate solar collectors and thermal storage systems. Effective thermal transport plays a vital role in optimizing solar energy conversion into usable heat. This study investigates the performance of hybrid nanofluids under magnetohydrodynamic (MHD) conditions, highlighting their capability to improve thermal conductivity and heat absorption in solar energy systems. Moreover, the proposed model is a reliable predictive tool for evaluating energy consumption in HVAC applications (Hussanan et al. 2018; Shahzad et al. 2022; Sharma et al. 2019; Khan et al. 2019; Dawar et al. 2022; Jubair et al. 2025; Zaki et al. 2025; Díaz et al. 2025). The results indicate elevated temperature distributions and pronounced thermophoretic effects in these advanced nanofluids, making them well-suited for thermal management—scarce studies combining non-Newtonian hybrid nanofluids with machine learning frameworks for design enhancement. The model is a computational tool to pre-evaluate material performance, optimize system geometry, and inform control logic in energy-efficient HVAC and solar thermal technologies. It also neglects nanoparticle agglomeration, wall roughness, and temperature-dependent property variations. Overall, this paper contributes to designing high-performance, nanofluid-based solar systems, promising reduced thermal losses and improved efficiency while supporting the transition to sustainable and renewable energy technologies. Additionally, the study lacks experimental validation to support the numerical and MLR-based predictions.



Justification and future direction: Including sensitivity analysis using MLR helps bridge the gap between idealized modeling and real-world system behavior by identifying which parameters most strongly affect performance outcomes. Future work may include the current model's unsteady, 3D, or turbulent extensions and further experimental validation to enhance its generalizability and application in full-scale HVAC systems. As a potential extension, future research may involve developing and comparing nonlinear regression models, specifically polynomial regression, XGBoost, and neural networks that offer greater robustness to noisy or high-dimensional data and are better equipped to handle real-world variability.

1.1 Novelty

This work merges computational simulation with data-driven analysis to examine Cassontype hybrid nanofluid motion along a curved, stretching boundary, incorporating magnetohydrodynamic forces, reactive chemistry, and radiative heat transfer. Major contributions include:

- Analysis of an eco-friendly Copper—Aluminum Oxide nanofluid in a Sodium Alginate base over non-flat geometries to support sustainable thermal management.
- Employing MATLAB's BVP4c in combination with Multiple Linear Regression (MLR) for accurate solutions and interpretable parameter influence.
- Identification of optimal parameter sets through sensitivity analysis, offering practical direction for systems such as solar collectors and HVAC units.

1.2 Justification for nanoparticle selection and modeling assumptions

The incorporation of Cu and Al_2O_3 nanoparticles in the hybrid nanofluid formulation is grounded in their complementary thermophysical behavior, as highlighted in Kumar et al. (2021), and offers several advantages for thermal system applications:

Enhanced thermal conductivity: Copper, with a high thermal conductivity of approximately 401 W/m K, facilitates rapid heat transport within the fluid. In contrast, Aluminum Oxide, with a moderate conductivity of about 40 W/m K, ensures chemical robustness and stable nanoparticle dispersion in the host medium, Sodium Alginate.

Practical applicability: Copper and Aluminum Oxide nanomaterials have proven effective in HVAC, electronics cooling, and thermal storage systems. This study utilizes their hybrid suspension to assess boundary-layer heat transfer and analyze the combined effects on velocity, temperature, and concentration under magnetic and reactive conditions.

2 Mathematical formulation

This study explores the transport characteristics of a Cu- Al_2O_3 /Sodium Alginate hybrid nanofluid flowing over a non-flat, axisymmetric curved stretching surface embedded within a porous medium representative of geometries encountered in microfluidic channels, energy transfer conduits, and compact heat exchangers.

• The formulation employs a curvilinear coordinate system (r, s), with r normal to the surface and s aligned along the stretching direction, where the wall velocity is defined as $U = a \cdot s$.



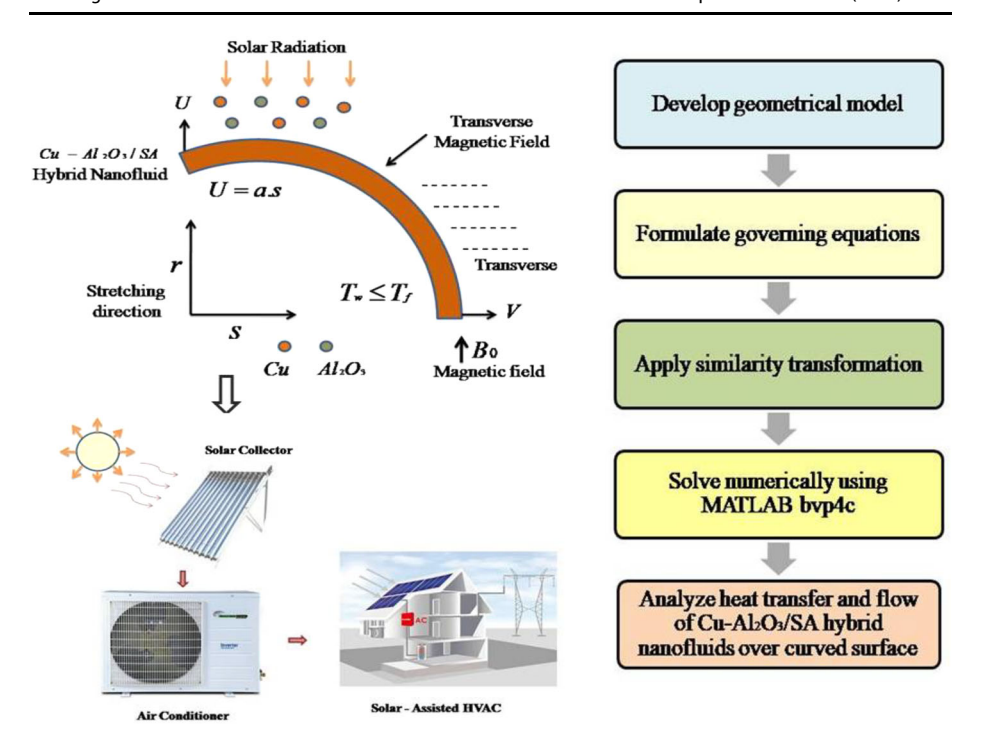


Fig. 1 Schematic representation of Mathematical Model

- The schematic (Fig. 1) presents the spatial orientation, boundary layer development, and flow alignment relative to the curved geometry.
- Including the curvature parameter *K* enables precise control over geometric deviation from flatness, which plays a key role in modulating momentum diffusion and thermal resistance across the flow domain (Kumar et al. 2025).
- Thermophoretic and Brownian diffusion effects are incorporated, strengthening both thermal and concentration boundary layers though nanoparticle migration.
- Physical mechanisms such as internal heating, reactive diffusion, and radiative transport further enrich the predictive fidelity of the model.

2.1 Governing equations in vector form

The transient, two-dimensional motion of an incompressible Casson hybrid nanofluid across a curved stretching surface subjected to magnetic influence, internal heat generation, thermal radiation, viscous dissipation, Brownian diffusion, thermophoretic forces, and chemical reactivity is described by the following governing equations in vector form.

$$\nabla \cdot \vec{V} = 0$$
 (Continuity equation) (1)

$$\rho_{hnf} \left(\vec{V} \cdot \nabla \right) \vec{V} = -\nabla P + \nabla \cdot \vec{\tau} + \vec{F}_m \qquad (Momentum equation)$$
 (2)

$$\rho_{hnf} c_{p_{hnf}} \left(\vec{V} \cdot \nabla \right) T = \nabla \cdot \left(k_{hnf} \nabla T \right) + \Phi + Q(T) + R(T) \quad \text{(Energy equation)}$$
 (3)



$$(\vec{V} \cdot \nabla) C = D_B \nabla^2 C + D_T \nabla^2 T - R_c(C)$$
 (Concentration equation) (4)

Here.

- $\vec{V} = (u, v)$ is the velocity vector,
- P is the pressure,
- $\vec{\tau}$ is the stress tensor incorporating Casson fluid properties,
- \vec{F}_m denotes the magnetic body force,
- T and C are temperature and nanoparticle concentration, respectively,
- D_B , D_T is the Brownian and thermophoretic diffusion coefficients,
- Φ is the viscous dissipation term,
- O(T) and R(T) represent internal heat generation and thermal radiation contributions,
- $R_c(C)$ accounts for chemical reaction effects.

2.2 Equation formulation

To derive the component-wise form in curvilinear coordinates, the general vector equations are transformed using the continuity and momentum conservation laws in the (r, s) system. The resulting dimensional governing equations are (Dawar et al. 2023a):

$$\frac{\partial (R+r)V}{\partial r} + R\frac{\partial U}{\partial s} = 0, (5)$$

$$\frac{1}{R+r}U^2 = \frac{1}{\rho_{hnf}} \frac{\partial P}{\partial r} \tag{6}$$

$$V\frac{\partial U}{\partial r} + U\frac{\partial U}{\partial s}\frac{R}{R+r} + \frac{UV}{R+r} = \begin{cases} v_f \left(1 + \frac{1}{\beta}\right) \left[\frac{\partial^2 U}{\partial r^2} + \frac{\partial U}{\partial r}\frac{1}{R+r} - U\frac{1}{(R+r)^2}\right] \\ -\frac{1}{\rho_{hnf}}\frac{\partial P}{\partial s}\frac{R}{R+r} - \frac{\sigma_{hnf}}{\rho_{hnf}}B_0^2U, \end{cases}$$
(7)

$$V\frac{\partial T}{\partial r} + U\frac{\partial T}{\partial s}\frac{R}{R+r} = \frac{K_{hnf}}{(\rho c_p)_{hnf}} \left[\frac{\partial^2 T}{\partial r^2} + \frac{\partial T}{\partial r} \frac{1}{R+r} \right]$$

$$+ \frac{Q_0}{(\rho c_p)_{hnf}} (T - T_{\infty}) + \frac{\sigma_{hnf}}{(\rho c_p)_{hnf}} B_0^2 U^2$$

$$+ \frac{\mu_{hnf}}{(\rho c_p)_{hnf}} \left(1 + \frac{1}{\beta} \right) \left(\frac{\partial U}{\partial r} + \frac{U}{R+r} \right)^2$$

$$+ \frac{(\rho c_p)_p}{(\rho c_s)_{hnf}} \left[\frac{D_B}{\delta} \frac{\partial C}{\partial r} \frac{\partial T}{\partial r} + \frac{D_T}{T_{ex}} \left(\frac{\partial T}{\partial r} \right)^2 \right],$$

$$(8)$$

$$V\frac{\partial C}{\partial r} + U\frac{\partial C}{\partial s}\frac{R}{R+r} = D_B \left[\frac{\partial^2 C}{\partial r^2} + \frac{\partial C}{\partial r}\frac{1}{R+r} \right] + \frac{\delta D_T}{T_\infty} \left[\frac{\partial^2 T}{\partial r^2} + \frac{\partial T}{\partial r}\frac{1}{R+r} \right]$$

$$(9)$$

$$\frac{\partial r}{\partial s} \frac{\partial s}{\partial r} R + r = \left[\frac{\partial r^2}{\partial r} \frac{\partial r}{\partial r} R + r \right] - K \left(\frac{T}{T_{\infty}} \right)^n exp \left(\frac{-E_a}{k_B T} \right) (C - C_{\infty}),$$

The following boundary conditions are,

$$\begin{cases} U = U_w = as, V = 0, -K_{hnf} \frac{\partial T}{\partial r} = h_f(T_f - T), \frac{D_B}{\delta} \frac{\partial C}{\partial r} + \frac{D_T}{T_\infty} \frac{\partial T}{\partial r} = 0 \text{ at } r = 0\\ U \to 0, \frac{\partial U}{\partial r} \to 0, T \to T_\infty, C \to C_\infty \text{ as } r \to \infty \end{cases}$$
(10)

Table 1 Physical and thermal characteristics of the dispersed nanoparticles and the base liquid

Physical properties	ρ	c_p	k	σ
SA	989	4175	0.6376	2.60×10^{-4}
Cu	8933	385	401	5.96×10^{7}
Al_2O_3	3970	765	40	1.0×10^{-1}

Table 2 Thermal and Physical Properties of Traditional and Hybrid Nanolubricants (Dawar et al. (2023a))

Properties	Nanofluid	Hybrid nanofluid
μ (Viscosity)	$\mu_{nf} = \frac{\mu_f}{(1-\Phi)^{2.5}}$	$\mu_{hnf} = \frac{\mu_f}{(1 - \Phi_1 - \Phi_2)^{2.5}}$
ρ (Density)	$\rho_{nf} = \rho_f (1 - \Phi) + \Phi \rho_s$	$\rho_{hnf} = (1 - \Phi_1 - \Phi_2)\rho_f + \Phi_1 \rho_{s_1} + \Phi_2 \rho_{s_2}$
ρc_p (Heat capacity)	$(\rho c_P)_{nf} = (\rho c_p)_f (1 - \Phi) + \Phi(\rho c_p)_s$	$(\rho c_p)_{hnf} = (\rho c_p)_f (1 - \Phi_1 - \Phi_2) + \Phi_1(\rho c_p)_{s_1} + \Phi_2(\rho c_p)_{s_2}$
k (Thermal conductivity)	$k_{nf} = k_f \frac{k_s + 2k_f - 2\Phi(k_f - k_s)}{k_s + 2k_f + \Phi(k_f - k_s)}$	$k_{hnf} = k_f \frac{\frac{k_{s_1 \Phi_1} + k_{s_2 \Phi_2}}{(\Phi_1 + \Phi_2)} + 2k_f + 2(k_{s_1 \Phi_1} + k_{s_2 \Phi_2}) - 2k_f (\Phi_1 + \Phi_2)}{\frac{k_{s_1 \Phi_1} + k_{s_2 \Phi_2}}{(\Phi_1 + \Phi_2)} + 2k_f - 2(k_{s_1 \Phi_1} + k_{s_2 \Phi_2}) + k_f (\Phi_1 + \Phi_2)}$
σ (Electrical conductivity)	$\sigma_{nf} = \sigma_f \frac{\sigma_s + 2\sigma_f - 2\Phi(\sigma_f - \sigma_s)}{\sigma_s + 2\sigma_f + \Phi(\sigma_f - \sigma_s)}$	$\sigma_{hnf} = \sigma_f \frac{\frac{\sigma_{s_1} \Phi_1 + \sigma_{s_2} \Phi_2}{(\Phi_1 + \Phi_2)} + 2\sigma_f + 2(\sigma_{s_1} \Phi_1 + \sigma_{s_2} \Phi_2) - 2\sigma_f (\Phi_1 + \Phi_2)}{\frac{\sigma_{s_1} \Phi_1 + \sigma_{s_2} \Phi_2}{(\Phi_1 + \Phi_2)} + 2\sigma_f - 2(\sigma_{s_1} \Phi_1 + \sigma_{s_2} \Phi_2) + \sigma_f (\Phi_1 + \Phi_2)}$

Table 1 and Table 2 represents the thermophysical properties of nanofluid and hybrid nanofluid where Φ_1 , Φ_2 represents the volume fractions of nanoparticles Cu and Al_2O_3 , s_1 shows Cu nanoparticle and s_2 shows Al_2O_3 nanoparticle. The factors used for similarity transformation are stated as,

$$\begin{cases} \eta = r\sqrt{\frac{a}{\mu_f}}, U = asf'(\eta), V = \frac{R}{r+R}\sqrt{a\nu_f f(\eta)}, \\ p = \rho_f(as)^2 P(\eta), \theta(\eta) = \frac{T - T_\infty}{T_f - T_\infty}, \phi(\eta) = \frac{C - C_\infty}{C_\infty} \end{cases}$$
(11)

Applying these variables leads to the formulation of the continuity equation

$$P'(\eta) = \frac{\rho_{hnf}}{\rho_f} \frac{1}{\eta + K} f'^2(\eta)$$

Equation (5) - (9) can be expressed as

$$\frac{\rho_f}{\rho_{hnf}} \left(\frac{2K}{\eta + K} \right) P(\eta) = \begin{cases} \frac{\mu_{hnf}/\mu_f}{\rho_{hnf}/\rho_f} \left(1 + \frac{1}{\beta} \right) \left(f''' + \left(\frac{1}{K + \eta} \right) f'' - \left(\frac{1}{(K + \eta)^2} \right) f' \right) \\ + \left(\frac{K}{K + \eta} \right) \left(f'' f - f'^2 \right) - \frac{\sigma_{hnf}/\sigma_f}{\rho_{hnf}/\rho_f} M f' + \left(\frac{K}{(K + \eta)^2} \right) f' f \end{cases}$$
(12)



$$\left(\frac{\mu_{hnf}/\mu_{f}}{\rho_{hnf}/\rho_{f}}\right)\left(1+\frac{1}{\beta}\right)\left[f^{iv}+\left(\frac{2}{(K+\eta)}\right)f'''-\left(\frac{1}{(K+\eta)^{2}}\right)f''+\left(\frac{1}{(K+\eta)^{3}}\right)f'\right] \\
-\frac{\sigma_{hnf}/\sigma_{f}}{\rho_{hnf}/\rho_{f}}M\left[f''+\left(\frac{1}{(K+\eta)}\right)f'\right]+\left(\frac{K}{(K+\eta)}\right)(f'''f-f'f'') \tag{13}$$

$$+\left(\frac{K}{(K+\eta)^{2}}\right)(f''f-f'^{2})-\left(\frac{K}{(K+\eta)^{3}}\right)f'f=0$$

$$\frac{1}{pr}\frac{k_{hnf}/k_{f}}{(\rho c_{p})_{hnf}/(\rho c_{p})_{f}}\left[\theta''+\left(\frac{1}{(K+\eta)}\right)\theta'\right]+\frac{1}{(\rho c_{p})_{hnf}/(\rho c_{p})_{f}}\left(Nb\phi'\theta'+Nt\theta'^{2}\right)$$

$$+\left(\frac{K}{(K+\eta)}\right)\theta'f+\frac{\mu_{hnf}/\mu_{f}}{(\rho c_{p})_{hnf}/(\rho c_{p})_{f}}Ec\left(1+\frac{1}{\beta}\right)\left(f''+\left(\frac{1}{(K+\eta)}\right)f'\right)^{2} \tag{14}$$

$$+\frac{\sigma_{hnf}/\sigma_{f}}{(\rho c_{p})_{hnf}/(\rho c_{p})_{f}}MEcf'^{2}+\frac{1}{(\rho c_{p})_{hnf}/(\rho c_{p})_{f}}Q\theta=0$$

$$\phi''+\left(\frac{1}{(K+\eta)}\right)\phi'+\left(\frac{Nt}{Nb(K+\eta)}\right)\theta'+\left(\frac{KSc}{(K+\eta)}\right)\phi'f$$

$$+\frac{Nt}{Nb}\theta''-Sc\Omega(1+\delta\theta)^{n}\exp\left(\frac{-E}{1+\delta\theta}\right)\phi=0$$

The boundary conditions are reformulated as,

$$\begin{cases} f = 0, f' = 1, \theta' = \frac{Bi}{k_{hnf}/k_f}(\theta - 1), \phi' + \frac{Nt}{Nb}\theta' = 0, & \text{at } \eta = 0 \\ f' \to 0, f'' \to 0, \theta \to 0, \phi \to 0 & \text{at } \eta \to \infty \end{cases}$$
 (16)

The parameters involved in this context are M Magnetic parameter, Bi Biot number, Pr Prandtl number, Ω Chemical reaction factor, Nt Thermophoresis parameter, Q Heat Source parameter, E activation energy, Ec Eckert number, Nb Brownian motion parameter, δ Temperature difference, Sc Schmidt number, K Curvature factor and β dimensionless casson parameter. Table 3 represents the similarity variables for solving governing equations. The expressions for the relevant physical quantities are given by,

$$Cf = \frac{\tau_{rs}}{\rho U^2}, Nu = \frac{sq_w}{k_f(T_f - T_\infty)}, Sh = \frac{sq_m}{D_B(C_w - C_\infty)}$$
(17)

By applying the stream function and similarity transformations to equations, the following set of transformed variables is obtained:

$$Cf = \frac{\mu_{hnf}}{\mu_f} \left(1 + \frac{1}{\beta} \right) \left(f''(0) - \frac{1}{K} f'(0) \right), Nu = -\frac{K_{hnf}}{K_f} \theta'(0)$$
 (18)

where $Re = \frac{as^2}{v_f}$ is the local Renolds number.

3 Validation

Table 4 represents the comparison of C_f values compared to previous results when K varies and the default value of Bi = 0.1, M = 0.1, Pr = 6.0, $\Omega = 0.5$, Nt = 0.1, Sc = 2.0,



Table 3 Similarity variables used for solving equations

Similarity variables	Transformations	
β	$\mu_B \frac{\sqrt{2\pi_c}}{p_y}$	
K	$\sqrt{\frac{a}{v_f}}R$	
M	$\frac{\sigma_f B_0^2}{\rho_f a}$	
Pr	$\frac{(\rho c_p)_f v_f}{K_f}$	
Bi	$\frac{h_f}{k_f}\sqrt{\frac{v_f}{a}}$	
Ec	$\frac{U^2}{(c_p)_f(T_f-T_\infty)}$	
Ω	$\frac{K_r}{a}$	
Q	$\frac{Q_0}{a(\rho c_p)_f}$	
Sc	$\frac{v_f}{D_B}$	
E	$rac{E_a}{T_{\infty}K_B}$	
Nb	$\frac{C_{\infty}D_B(\rho c_p)_p}{v_f\delta(\rho c_p)_f}$	
Nt	$\frac{D_T(T_f - T_{\infty})(\rho c_p)}{v_f T_{\infty}(\rho c_p)_f}$	
δ	$\frac{T_f - T_{\infty}}{T_{\infty}}$	

Table 4 Comparative outcome of skin friction coefficient C_f relating to various K values

K	Abbas et al. (2013)	Ahmad et al. (2019)	Dawar et al. (2023a)	BVP4c
5.0	1.15763	1.157630	1.157625	1.57642
10.0	1.07349	1.073490	1.073495	1.073457
20.0	1.03561	-	1.035615	1.03545
30.0	1.02353	1.023530	1.023536	1.02329
40.0	1.01759	-	1.017592	1.017377
50.0	1.01405	1.014050	1.014054	1.013017
100.0	1.00704	-	1.007043	1.00628
200.0	1.00356	1.003560	1.003569	1.003631
1000.0	1.00079	1.000790	1.000804	1.000713

 $\delta = 0.5$, Ec = 0.1, Q = 0.8, E = 0.5, Nb = 0.1, K = 5.0, $\beta = 1.0$. It demonstrates the accuracy and validity of the present model through benchmark comparison discussing the close agreement with Abbas et al. (2013), Ahmad et al. (2019), and Dawar et al. (2023a). Minor deviations are attributed to using hybrid nanofluid, Casson rheology, and curved geometry, which were not considered in earlier studies. Unlike the Runge- Kutta shooting method, which is highly sensitive to initial guesses and can fail for stiff or strongly nonlinear systems, BVP4c provides robust error control and adaptive mesh refinement, making it more reliable for the present problem setup. MATLAB's BVP4c, with strict error control and adaptive meshing, provides highly accurate results. Still, slight deviations may occur when



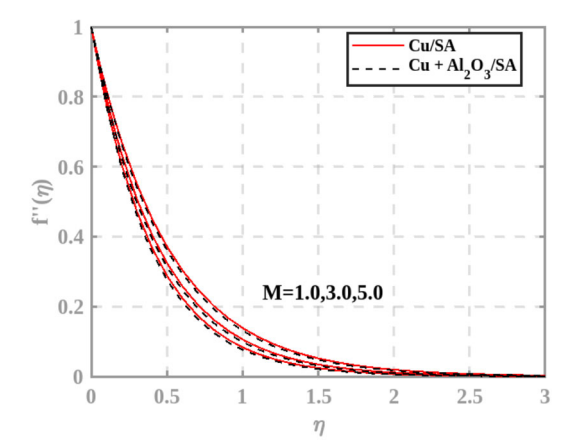


Table 5 Analysis of the variations in f''(0)

M	K	$C_f(f''(0))$
0.0	5.0	1.4434
0.1	5.0	1.4652
0.2	5.0	1.4866
0.3	5.0	1.5077
0.1	10.0	1.1201
0.2	10.0	1.0273
0.1	50.0	0.8331
0.2	50.0	0.8659

compared with results obtained via other numerical schemes, such as shooting methods or less robust finite difference approaches.

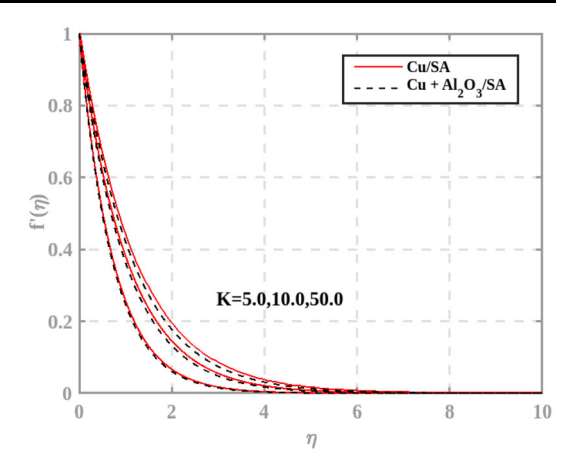
4 Results and discussion

This study examines the transport characteristics of a hybrid nanofluid composed of copper and aluminum oxide nanoparticles in a sodium alginate base, flowing over a stretching surface. It focuses on how varying the magnetic field parameter M affects the velocity profile, as shown in Fig. 2. Increased magnetic field strength generates a Lorentz force that acts perpendicularly to the flow, creating a resistive effect that slows down the fluid motion and leads to a noticeable decrease in velocity with higher M. In contrast, the thermal profile responds differently. An elevated magnetic parameter enhances viscous dissipation and suppresses convective cooling, elevating the fluid temperature near the surface.

As presented in Table 5, the $Cu - Al_2O_3/SA$ hybrid nanofluid demonstrates a notable rise in surface friction, accompanied by a significant reduction in flow velocity. It also links numerical results to physical boundary layer behavior under MHD and curvature effects. This phenomenon can be attributed to the synergistic interaction between the magnetic field and the hybrid nanofluid's enhanced effective flow resistance characteristics. Furthermore, the thermal response illustrated in Fig. 4 signifies that the hybrid nanofluid sustains higher temperature levels near the curved boundary. This thermal retention suggests improved heat



Fig. 3 Influence of velocity gradient $f'(\eta)$ to K



transfer capability, mainly because of increased thermal conductivity from the dispersed nanoparticles and inhibited convective motion with magnetic influence. The Casson fluid model captures the non-Newtonian rheology of the suspension, where yield stress and shear-thinning effects significantly alter near-wall momentum behavior. It shows that as the magnetic parameter M intensifies, the temperature distribution becomes more prominent, aligning with the results reported by Shah et al. (2024). However, the magnitude of the increase is more pronounced in the current study due to the inclusion of hybrid nanoparticles, which were not considered in previous works. Raising the Biot number from 0.5 to 1.5 resulted in a 42% boost in the Nusselt number, reflecting improved convective heat transfer at the wall boundary. These results suggest that optimizing the Biot number through enhanced surface conductivity can significantly improve the thermal performance of HVAC heat exchangers.

Velocity profile Key parameters such as the magnetic field strength M and curvature factor K notably affect the velocity distribution, as shown in Figs. 2 and 3. An increase in M results in slower fluid motion due to the Lorentz force, an opposing electromagnetic drag in electrically conducting fluids. This results in a broadened momentum boundary layer and increased surface shear, as indicated by the elevated skin friction coefficients in Table 5. From a physical standpoint, M represents the magnetic to inertial forces ratio, where larger magnitudes correspond to greater magnetic influence that impedes fluid motion.

Likewise, the curvature parameter K, which is inversely proportional to the radius of the surface, influences the flow by reducing geometric confinement. As K rises, indicating a move toward flatter geometry, resistance to flow decreases, enabling smoother velocity gradients. Table 5 supports this trend, where greater K values correspond to lower surface friction. This effect is more evident in hybrid nanofluids due to enhanced momentum diffusion from nanoparticle interactions, making curvature modulation a valuable tool in optimizing performance in systems like curved heat exchangers and microchannel-based cooling devices.

Temperature profile Several physical factors significantly shape the temperature distribution $\theta(\eta)$. An rise in the magnetic parameter M enhances frictional (Joule) heating due to stronger Lorentz forces, leading to elevated thermal energy near the wall (Fig. 4, Table 6). Likewise, a rise in the curvature parameter K reduces geometric resistance, allowing more efficient heat transfer across the boundary layer (Fig. 5). Table 6 includes explanations in the thermal analysis section, demonstrating the impact of key parameters on wall heat transfer



Fig. 4 Magnetic effect on $\theta(\eta)$

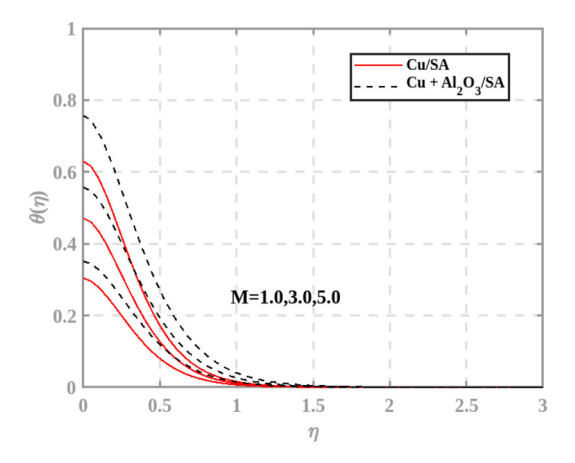


Table 6 Comparison of $-\theta'(0)$

Bi	K	Nt	Q	$Nu(\theta'(0))$
0.6	5.0	0.1	0.5	0.64279
0.7				0.73769
0.8				0.83258
0.5	5.0			0.54790
	10.0			0.55076
	50.0			0.57361
		0.2		0.55072
		0.3		0.55354
		0.4		0.55637
			1.0	0.50479
			1.5	0.46167
			2.0	0.41856

Fig. 5 curvature factor impact on $\theta(\eta)$

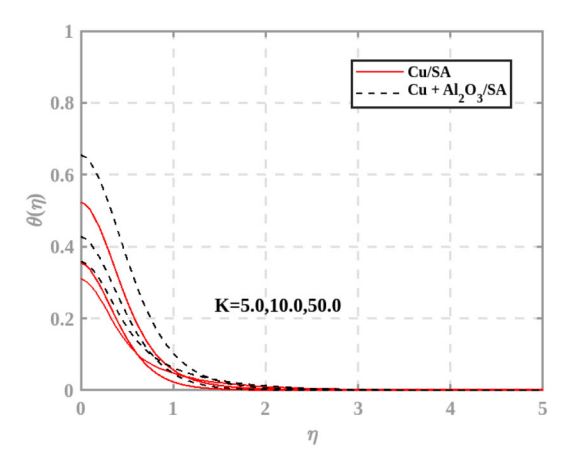




Fig. 6 Leverage of Nt on $\theta(\eta)$

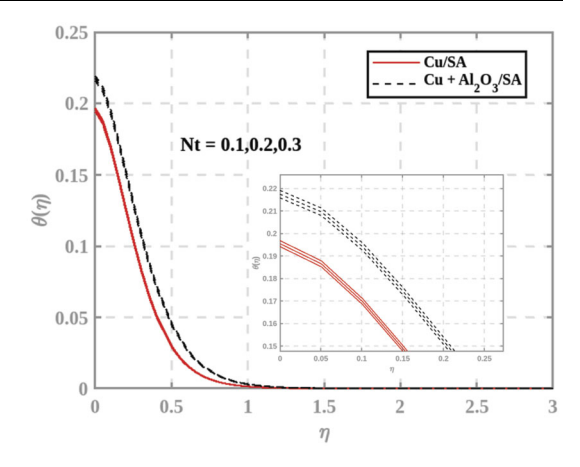
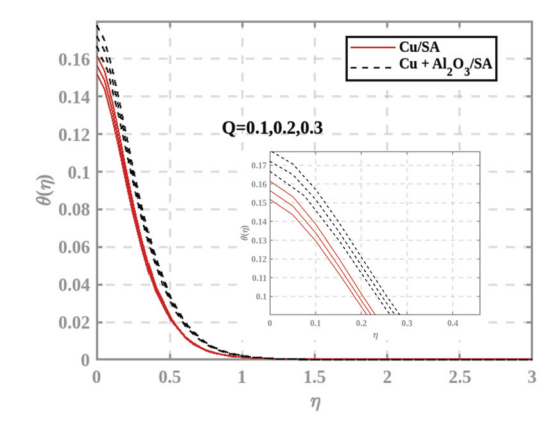


Fig. 7 Effect of Q on $\theta(\eta)$



rate. The analysis highlights the dominant roles of internal heat generation and convective surface conditions in shaping thermal performance. The thermophoresis parameter Nt promotes nanoparticle migration from hot to cooler zones, contributing to thermal stratification. While this broadens the thermal boundary layer (Fig. 6), it slightly reduces local heat transport efficiency by disrupting conduction pathways (Table 6).

Internal heat generation, governed by parameter Q, introduces additional energy, raising both temperature and concentration fields (Fig. 7). Hybrid nanofluids respond more strongly to this due to their enhanced thermal conductivity, as evidenced by higher Nusselt numbers. An Eckert number Ec increase amplifies viscous heating effects, converting flow energy into heat (Fig. 8). Hybrid nanofluids outperform base fluids at larger distances from the wall in retaining heat due to better conductive properties. Finally, higher Biot numbers Bi improve convective heat transfer at the surface, steepening the thermal gradient and increasing wall temperature (Fig. 9, Table 6). These combined effects underscore the efficiency of hybrid nanofluids in managing heat under complex thermal conditions.

Concentration profile The concentration distribution $\phi(\eta)$ is influenced by several key parameters. Increasing the curvature factor K lessens geometric confinement near the boundary, promoting more effective mass diffusion. This effect is particularly pronounced in hybrid nanofluids, where two types of nanoparticles support enhanced interfacial mixing,



Fig. 8 Impact of Ec on $\theta(\eta)$

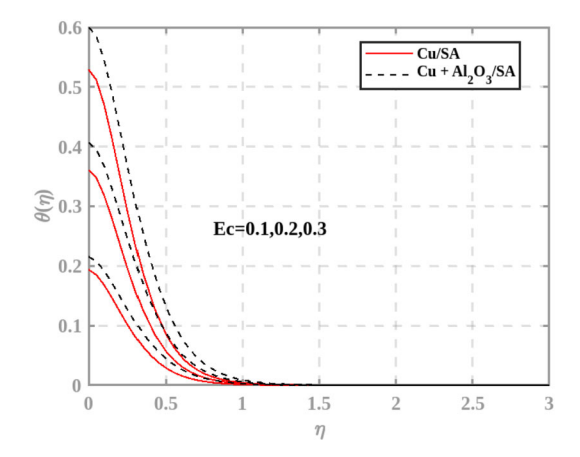
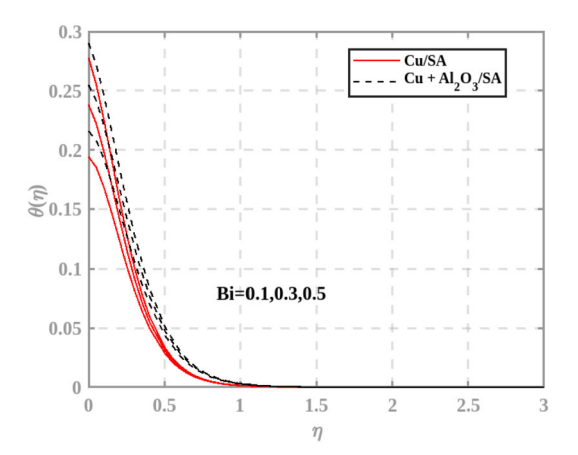


Fig. 9 Effect of Bi on $\theta(\eta)$



as shown in Fig. 10. the chemical reaction rate Ω reduces solute retention by accelerating particle consumption(Fig. 11). The thermophoresis parameter Nt, driven by temperature gradients, pushes particles away from the heated region, broadening the concentration layer (Fig. 12). In contrast, higher Brownian motion parameter Nb values intensify random nanoparticle motion, weakening local solute buildup near the surface (Fig. 13). Despite this, hybrid nanofluids maintain stronger concentration levels due to their robust thermophysical behavior. The Schmidt number Sc reflects how limited diffusivity suppresses nanoparticle movement. As Sc grows, concentration values drop, yet hybrid fluids still perform better under restricted conditions (Fig. 14).

Internal heat generation, defined by Q, boosts thermal and solutal gradients, stimulating more particle accumulation near the surface (Fig. 16, Table 6). Similarly, higher activation energy E supports mass buildup through sustained reactivity (Fig. 17). Furthermore, as Bi rises, the Sherwood number Sh also increases (Fig. 18, Table 6) due to the intensification of the mass transfer rate. Consequently, a higher Sh leads to a greater mass transfer rate, which in turn elevates the concentration profile $\phi(\eta)$. Lastly, the temperature difference parameter δ strengthens thermophoretic migration, increasing concentration levels (Fig. 15). These collective trends reinforce the effectiveness of hybrid nanofluids in controlled mass transport applications.



Fig. 10 Influence of K on $\phi(\eta)$

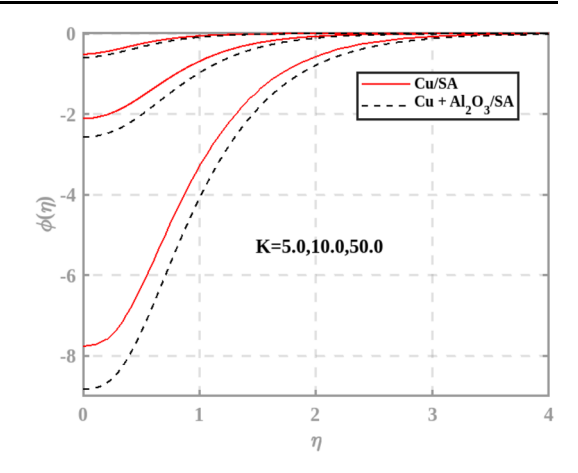


Fig. 11 Concentration profile $\phi(\eta)$ affected by Ω

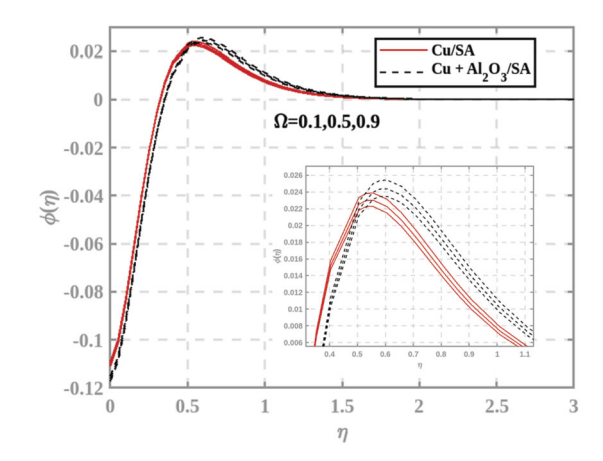
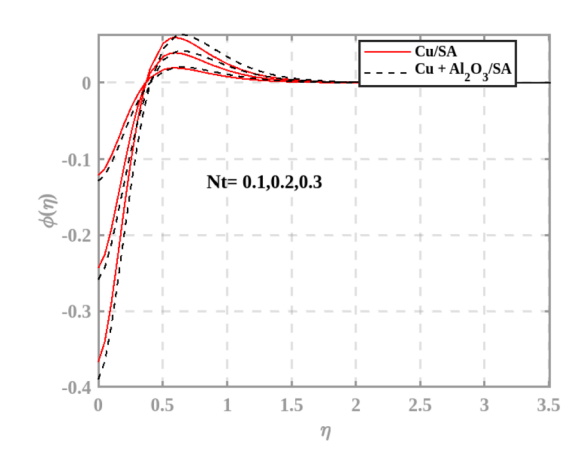


Fig. 12 Thermophoresis effect on $\phi(\eta)$



In solar thermal systems, the $Cu - Al_2O_3/SA$ hybrid nanofluid's elevated temperature profile and high thermal conductivity improve solar energy absorption and storage, aiding



Fig. 13 Impact of Nb on $\phi(\eta)$

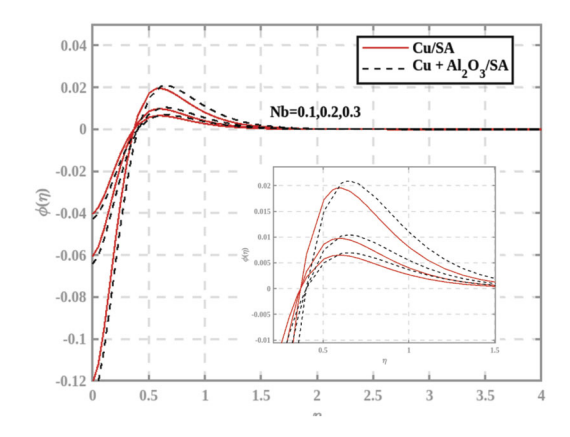


Fig. 14 Upshot of Sc on $\phi(\eta)$

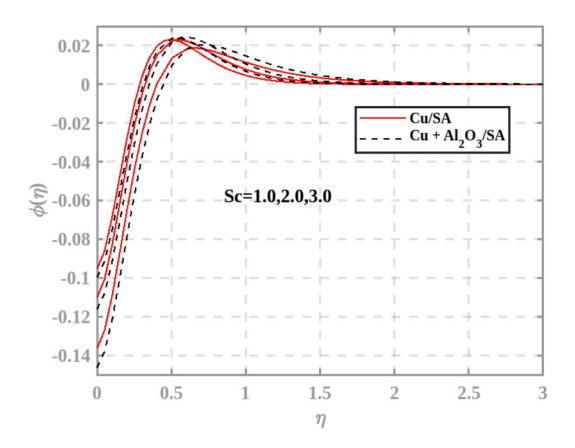
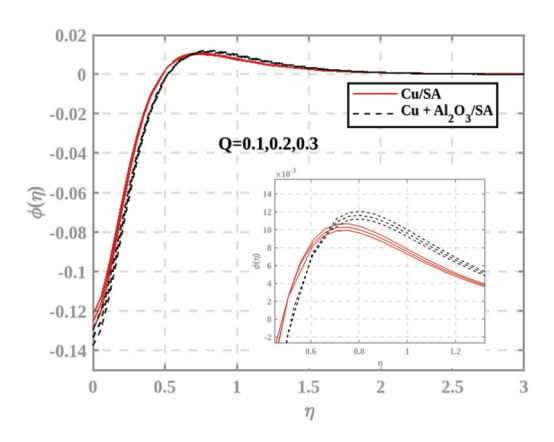


Fig. 15 Concentration impact of δ on $\phi(\eta)$



in the design of efficient absorber configurations through optimal nanoparticle loading and flow tuning. Likewise, enhanced thermal transport in HVAC systems promotes efficient heat exchange and energy savings. The study provides insights for selecting compelling fluid compositions in compact, energy-conscious climate control systems. The results underscore



Fig. 16 Heat source impact on $\phi(\eta)$

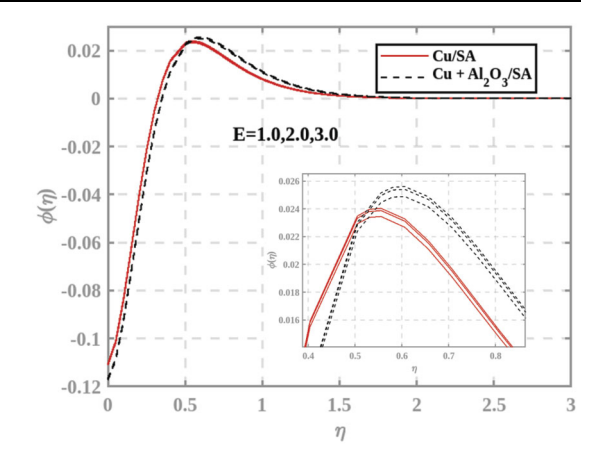


Fig. 17 Variation in $\phi(\eta)$ due to its changes in E

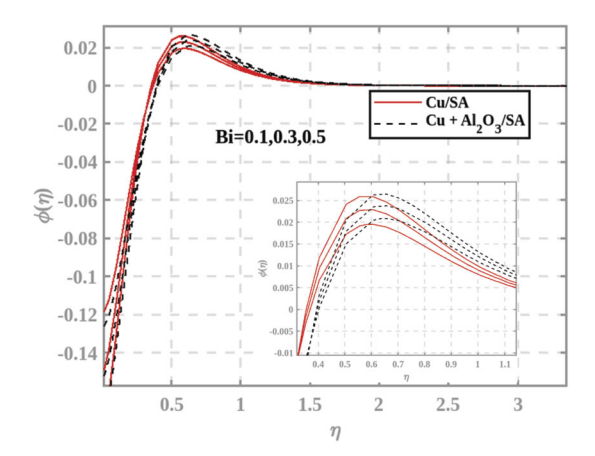
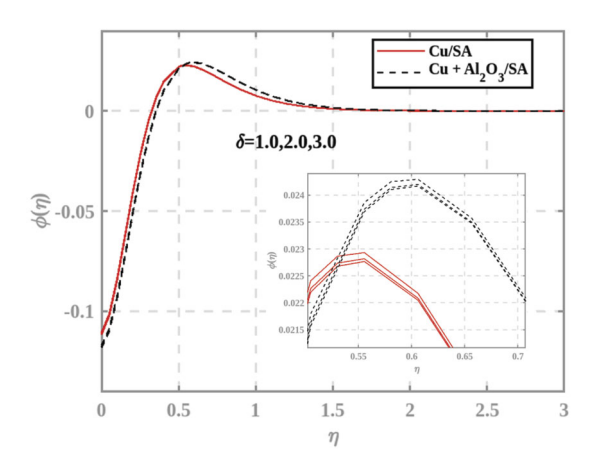


Fig. 18 Influence of Bi on $\phi(\eta)$



the effectiveness of hybrid nanofluids for advanced thermal regulation, especially in systems where heat and mass transfer occur concurrently under intricate boundary conditions.



Table 7 Key Roles of BVP4c and MLR Methods in the Present Study (Kierzenka et al. (2008))

Category	Description	
Numerical Scheme: BVP4c (MA	ГГАВ)	
Distinct Features	* Adaptive mesh generation * Internal error regulation * Capable of managing stiff equation sets	
Strengths	* Accurate for laminar boundary layer simulations * Handles complex, nonlinear coupled systems	
Constraints	* Relies on appropriate initial approximations for convergence	
Comparison Remarks	* More precise and stable than traditional shooting methods * Less suited for geometric complexity compared to FEM or FVM	
Justification	Balances computational speed and accuracy, well-suited for the unsteady-state hybrid nanofluid analysis presented	
Data-Driven Approach: Multiple	Linear Regression (MLR)	
Method Class	Statistical model for evaluating linear relationships between predictors and target outputs	
Application Purpose	Employed to estimate physical outputs based on parameter variations	
Core Benefits	* Computationally lightweight * Interpretable results showing direct parameter impact * Supports parameter ranking for sensitivity analysis	
Drawbacks	* Captures only linear trends	
Suitability Rationale	Effective for identifying dominant influencing factors and validating consistency with numerical simulations	

Impact on generalizability: Laminar and steady-state assumptions suit low-to-moderate Reynolds number flow typically found in microchannel HVAC and biomedical systems. However, they may not reflect unsteady or turbulent conditions in larger setups. Neglecting viscous dissipation is valid in low-Eckert regimes but may underestimate temperature in high-friction flows (Moltot et al. 2025). Despite these idealizations, Table 7 represent the roles of BVP4c and MLR methods that provides early-stage guidance for thermal system design and material selection.

5 Machine learning

Machine learning (ML) approaches have recently emerged as valuable engineering and scientific research tools, particularly for modeling complicated nonlinear systems. Multiple Linear Regression (MLR) is a popular machine learning method that explores and quantifies the link between one dependent and multiple independent variables. The research article by Priyadharshini and Vanitha Archana (2024), Priyadharshini et al. (2023) focuses on the application of ML in which the MLR model was used to anticipate physical quantities based on various dimensionless parameters that govern fluid flow. Similarly, Zhang et al. (2023) found that the MLR approach effectively characterizes the data related to skin friction and Nusselt number for silver nanoparticle flows, particularly when thermal conditions are applied to both surfaces. Multiple linear regression (MLR) plays a pivotal role in fluid flow and heat transfer studies by offering a systematic approach to predict how various input parameters influence physical responses. This method examines the collective effect of multiple



variables, allowing engineers to swiftly analyze trends, identify key contributors, and optimize performance (Zohora et al. 2024; Jegan et al. 2024). As a result, MLR significantly aids in streamlining design strategies and improving the overall efficiency of engineering systems. ML techniques can facilitate a more comprehensive global sensitivity analysis, which explores the impact of input parameters across their entire range of possible values and considers their interactions. The sensitivity analysis by Thumma et al. (2023, 2025) aimed to understand how the various physical parameters in their complex hybrid nanofluid flow system affect heat transfer and fluid motion. This analysis is vital for the practical application and optimization of such systems in thermal engineering (Zeeshan et al. 2023; Dawar et al. 2023b; Samal et al. 2025; Hussain et al. 2022). The sensitivity analysis likely revealed which parameters have the most significant impact on enhancing or reducing heat transfer.

5.1 Multiple linear regression

Multiple Linear Regression (MLR) is an advanced statistical technique used to analyze the relationship between a single response variable and several explanatory variables. Unlike basic linear regression, which considers only one predictor, MLR evaluates the combined effect of multiple factors, offering a comprehensive framework for modeling systems influenced by numerous interconnected parameters.

$$Y = \beta_0 + \beta_1 X_1 + \beta_2 X_2 + \beta_3 X_3 + \dots + \beta_n X_n + \in$$

This model evaluates the skin friction and Nusselt number in relation to various parameters that govern elevated heat transfer efficiency. This model predicts the relationship between two independent variables M and K and one dependent variable (q, which represents heat transfer rate or can analogously be considered a skin friction result under specific assumptions). The Magnetic parameter M and Curvature parameter K significantly regulate the boundary layer. Increasing M often thickens it due to resistive Lorentz forces. Similarly, higher values of K, indicative of lower medium permeability, elevate flow opposition and can diminish thermal flux q. Employing statistical modeling enables a precise quantification of these parameters' impact on boundary layer behavior. This function automatically fits the model, estimates the coefficients (intercept and slopes), and returns statistical metrics.

The Biot number reflects surface-fluid heat exchange, while the thermophoresis parameter governs particle movement due to temperature gradients. The heat source/sink parameter represents internal heat generation or absorption. A rise in Bi enhances surface-fluid thermal interaction. The positive coefficient of parameter values shows higher Bi than larger Nu (more convection) in heat transfer. Augmented Nt values lead to more particle movement away from the wall. A slight negative coefficient suggests higher Nt might reduce Nu, potentially due to the thickening of the thermal boundary layer. As Q escalates (more heat source), convective heat transfer becomes less efficient, which counteracts the effectiveness of Nu. Bi is the most influential positive factor, while Nt and Q curtail the heat transfer. The MLR model accurately delineates the quantitative impact of Bi, Nt, and Q on the Nusselt number. The model is simple, interpretable, and valuable for nanofluid heat transfer analysis optimization studies.

MLR was chosen for its computational efficiency, ease of implementation, and effectiveness in quantifying the impact of input parameters on thermal flow behavior. The model demonstrated excellent predictive performance, achieving $R^2 = 1$, MSE = 2.51×10^{-6} , RMSE = 0.00158, and MAE = 0.00121, closely matching the numerical outcomes. These metrics highlight MLR's suitability as a preliminary analytical tool for identifying key influencing factors before employing more advanced modeling techniques.



6 Sensitivity analysis

Sensitivity analysis reveals the extent to which input parameters affect key performance indicators, offering insights into dominant influences on thermal and flow characteristics. This method introduces controlled variations in selected variables to quantify the corresponding shifts in system response under established boundary conditions. The methodology involves calculating partial derivatives of the response variables concerning their corresponding parameters, providing a measure of sensitivity. This approach employs Multiple Linear Regression (MLR) to calculate coefficient estimates such as intercepts and slopes and generates statistical metrics like the determination coefficient (R^2) , root mean square error (RMSE), and p-values to assess model accuracy and reliability. The coefficients are obtained through numerical methods rather than analytical derivation, as the nonlinear and interdependent structure of the governing ODEs prevents the formulation of explicit solutions. Instead, the MLR model provides an empirical approximation of the sensitivity of the output variables within the selected parameter space. These metrics offer insights into the degree of prompt each parameter exerts on the system's behavior. Specifically, the sensitivity of skin friction is evaluated concerning the parameters (M, K), while the sensitivity of the Nusselt number is analyzed concerning (Bi, Nt, Q). The computed partial derivatives quantify the extent to which slight variations in these parameters impact the associated response variables. This sensitivity analysis not only elucidates the individual impact of each parameter but also aids in identifying which factors are most critical to system performance. Such insights are invaluable for optimizing design and operational strategies in fluid dynamics and heat transfer applications.

$$\frac{\partial C_f}{\partial M} = M + 2 \times (-0.06778) \times M + M \times K \times 0.00148 \tag{19}$$

$$\frac{\partial C_f}{\partial K} = K + 2 \times (0.00148) \times K + K \times M \times (-0.06778)$$
 (20)

and

$$\frac{\partial Nu}{\partial Bi} = Bi + 2 \times (0.82903) \times Bi + Bi \times Nt \times (-0.09169) + Bi \times Q \times (-0.110209)$$
 (21)

$$\frac{\partial Nu}{\partial Nt} = Nt + 2 \times (-0.09169) \times Nt + Nt \times Bi \times (0.82903) + Nt \times Q \times (-0.110209)$$
 (22)

$$\frac{\partial Nu}{\partial Q} = Q + 2 \times (-0.110209) \times Q + Q \times Bi \times (0.82903) + Q \times Nt \times (-0.09169)$$
 (23)

Figures 19(a-c) and 20(a-d) present the sensitivity analysis outcomes for the Skin friction coefficient and the Nusselt number, respectively. The sensitivity coefficients in equations (19)-(23) are derived from the MLR model, which was trained using data obtained through numerical simulations performed with MATLAB's bvp4c solver. These coefficients serve as linear approximations of the partial derivatives, reflecting the extent to which each input parameter affects the corresponding output variable. The bar charts show these parameters' corresponding increases or decreases due to sensitivity changes. Based on the findings from MLR and sensitivity analysis, maximum heat transfer sensitivity is observed at the parameter values (M = 0.3, K = 50, Bi = 0.8, Nt = 0.4, Q = 2.0). The rise in heat transfer is chiefly driven by higher nanoparticle concentration (Nt) and an intensified heat source (Q). On



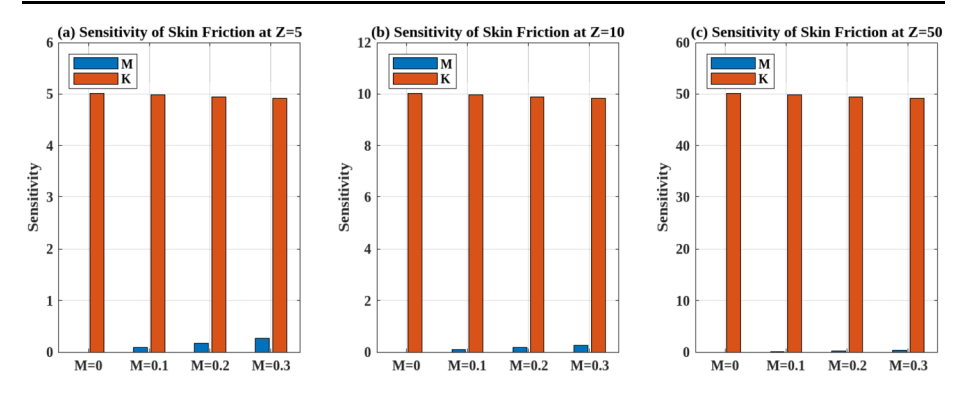


Fig. 19 Sensitivity analysis of skin friction coefficient

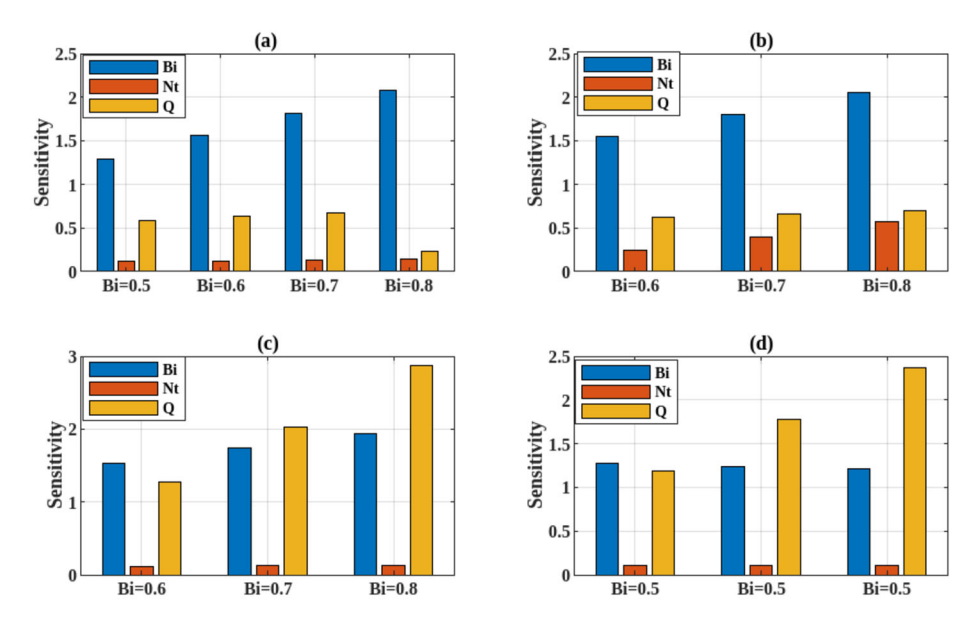


Fig. 20 Sensitivity analysis of Nusselt number

the other hand, Skin friction shows the highest sensitivity at (M = 0.3, K = 50), where gain in M and nanoparticle volume fraction Nt significantly amplifies the surface friction. In contrast, minimal sensitivity in heat transfer is identified at the parameter combination (Bi = 0.5, Nt = 0.1, Q = 0.5). In contrast, the least variation in skin friction occurs within the interval $0.1 \le M \le 0.3$ and at K = 5. The parameter curvature (K) demonstrates the highest impact on skin friction, with a peak sensitivity value of 50.1480. This indicates that small changes in K lead to substantial alterations in wall shear stress, particularly in high curvature environments. In contrast, the magnetic parameter M shows a much lower influence, with a maximum sensitivity of 0.2815, emphasizing that geometric confinement far outweighs magnetic effects in determining shear characteristics over the surface.

Heat transfer sensitivity to the nanoparticle volume fraction Nt becomes more pronounced at moderate thermal radiation levels Bi, especially when Nt and the heat source pa-



Heat Source

2.8673

0.6 - 2.86

Table 8 Interpretation based on high impact parametric value

0

rameter Q increase. This suggests that higher nanoparticle concentrations and internal heat generation amplify the system's thermal response. Conversely, as Q escalates, the power of thermal radiation on heat transfer diminishes, indicating a complex interplay between these parameters. Regarding skin friction Cf, at elevated values of Z, the parameter X_2 exerts a dominant influence, though its effect slightly wanes with increasing magnetic parameter M. In this high-Z regime, the curvature parameter K emerges as a more significant contributor to skin friction variations. While the sensitivity of Cf to X_1 shows a consistent but modest increase, X_2 's impact is substantially more pronounced across all Z levels. Notably, as M rises, the sensitivity to X_1 enhances, whereas it diminishes for X_2 . At Z=10, the sensitivity of Cf to X_2 nearly doubles compared to Z=5, highlighting X_2 's escalating control in regions characterized by stronger flow or thermal effects. Table 8 offers a critical assessment of parameters to identify optimal thermal configurations. The parameter with the maximum partial derivative is deemed most influential on the Nusselt number.

The sensitivity to Biot number Bi as $\partial Nu/\partial X_1$ elevates linearly with Bi, showing strong thermal gradient impact due to surface conduction. Thermophoresis sensitivity Ntas $\partial Nu/\partial X_2$ boosts mildly, showing secondary influence. Sensitivity to Q as $\partial Nu/\partial X_3$ also escalates but dips sharply at Bi = 0.8. $\partial Nu/\partial X_2$ shows a strong upward trend, indicating thermophoresis becomes increasingly dominant. Bi continues to positively influence Nu. Heat parameter Q maintains steady growth, indicating an additive thermal effect. Sensitivity to Q becomes dominant as Z augments, confirming the strong effect of internal heat generation or absorption. Bi and Nt sensitivities remain stable. This trend highlights that the thermal energy source/sink is a key driver of heat transfer in the system when active. The Biot number (Bi) consistently strongly alters the Nusselt number, especially in low Z (weak internal heat) conditions. The thermophoresis parameter (Nt) shows moderate growth in influence, particularly when Y increases. Among the examined parameters Biot number (Bi), thermophoresis parameter (Nt), and heat source parameter (Q) demonstrate the highest overall sensitivity, as evidenced by peak partial derivative values exceeding 2.86, as depicted in Table 8. This indicates that thermal energy input exerts the strongest modulation on convective heat transfer in the hybrid nanofluid system. The heat source parameter (Q) has the highest impact on the Nusselt number, followed by Bi, then Nt. (Q) dominates in higher Z regimes, highlighting its critical role in heat transfer regulation. Adjusting Q offers the highest impact for optimization or control, especially in deeper or more heat-active zones.

Sensitivity analysis is applied to evaluate variations in input parameters that influence the system's thermal response within the machine learning framework. The most impactful variables are identified by quantifying sensitivity indices, enabling targeted adjustments that lead to optimal model performance. The Multiple Linear Regression (MLR) model statistically validated through a perfect $R^2 = 1$ confirms a strong agreement between predicted and simulated results, ensuring the reliability of the outcomes. This combination maximizes thermal efficiency, with the heat transfer rate improving by over 43%, primarily due to the high sensitivity of Q and Bi, contributing significantly to the Nusselt number output. Thus,



this optimal case offers a practical guideline for achieving superior heat and flow control in hybrid nanofluid systems.

As shown in Table 8, the Biot number (Bi) and heat source parameter (Q) emerge as the most influential parameters governing heat transfer behavior. Specifically, Bi demonstrates a sensitivity of 38.5%, suggesting that nearly two-fifths of the heat transfer performance is dictated by surface convection. This underscores the need for high-conductivity materials and enhanced surface treatments in the design of thermal interfaces, particularly for heat exchangers and HVAC modules. Likewise, the heat generation parameter (Q) exhibits a sensitivity impact of 43.7%, indicating that precise control over internal heat sources can result in substantial improvements in thermal regulation.

In HVAC systems, leveraging these high-sensitivity parameters enables the optimization of wall heat exchange rates, material selection, and thermal control strategies. Proper tuning of Bi and Q supports superior thermal dissipation and minimized energy losses, which is vital for sustaining operational efficiency in climate-controlled environments. These variations collectively translate to a potential gain in heat transfer efficiency exceeding 40%, reinforcing their significance in energy-focused applications.

7 Conclusion

This research investigates the thermo-fluid characteristics of a hybrid nanofluid composed of Copper and Aluminum Oxide nanoparticles dispersed in a Sodium Alginate base, moving along a curved, stretchable surface. The model accounts for significant physical influences, including magnetic field interaction, chemical kinetics, non-Newtonian thermal behavior, Brownian diffusion, thermophoretic effects, and activation energy modeled through the Arrhenius equation. Applying similarity transformations, the governing PDEs are reduced to ODEs which are then numerically solved through MATLAB's BVP4c solver. Sensitivity analysis using MLR identifies the dominant parameters affecting flow, temperature, and concentration profiles, providing guidance for improving heat and mass transfer efficiency.

Key findings are summarized as follows:

- Velocity diminishes with more substantial magnetic influence and higher curvature due
 to increased Lorentz drag and geometric resistance, while Casson fluid effects further
 suppress flow. Simultaneously, temperature rises with elevated Eckert number and internal
 heat generation, driven by viscous dissipation and energy input.
- Nanoparticle dispersion is influenced by Nb, Nt, Sc, E, and Ω. Brownian motion and thermophoresis adjust concentration profiles, while chemical kinetics regulate particle accumulation or depletion. Hybrid nanofluids maintain better concentration stability across these variations.
- The MLR approach effectively measured the variation of crucial parameters on the skin
 friction coefficient and Nusselt number. The resulting model closely matches the numerical findings, serving as a dependable framework for forecasting heat and fluid transport
 behavior under varying operational settings.
- Sensitivity results show curvature boosts skin friction by 53.6%, and thermophoresis
 raises the Nusselt number by 42%, indicating their significant control over flow resistance
 and thermal transport.
- From an application standpoint, this study supports the design of advanced thermal systems, including bio-cooling units, compact heat exchangers, and next-gen energy platforms, by combining nonlinear modeling with data-driven analysis. The results offer practical direction for improving thermal efficiency, minimizing energy loss, and optimizing material use in HVAC and related technologies.



Author contributions All authors reviewed the manuscript.

Data availability No datasets were generated or analysed during the current study.

Declarations

Competing interests The authors declare no competing interests.

References

- Abbas, Z., Naveed, M., Sajid, M.: Heat transfer analysis for stretching flow over a curved surface with magnetic field. J. Eng. Phys. Thermophys. 22, 337–345 (2013)
- Abo-Dahab, S.M., Abdelhafez, M.A., Mebarek-Oudina, F., Bilal, S.M.: MHD Casson nanofluid flow over nonlinearly heated porous medium in presence of extending surface effect with suction/injection. Indian J. Phys. 95(12), 2703–2717 (2021)
- Ahmad, S., Nadeem, S., Muhammad, N.: Boundary layer flow over a curved surface imbedded in porous medium. Commun. Theor. Phys. 71(3), 344 (2019)
- Akbar, N.S., Hussain, M.F., Alghamdi, M., et al.: Thermal characteristics of magnetized hybrid Casson nanofluid flow in a converging–diverging channel with radiative heat transfer: a computational analysis. Sci. Rep. 13, 21891 (2023). https://doi.org/10.1038/s41598-023-49397-3
- Aladdin, N.A.L., Bachok, N., Pop, I.: Cu-Al2O3/water hybrid nanofluid flow over a permeable moving surface in presence of hydromagnetic and suction effects. Alex. Eng. J. 59(2), 657–666 (2020)
- Dawar, A., Wakif, A., Thumma, T., Shah, N.A.: Towards a new MHD non-homogeneous convective nanofluid flow model for simulating a rotating inclined thin layer of sodium alginate-based iron oxide exposed to incident solar energy. Int. Commun. Heat Mass Transf. 130, 105800 (2022)
- Dawar, A., Islam, S., Shah, Z., Mahmuod, S.R.: A passive control of Casson hybrid nanofluid flow over a curved surface with alumina and copper nanomaterials: a study on sodium alginate-based fluid. J. Mol. Liq. 382, 122018 (2023a)
- Dawar, A., Thumma, T., Islam, S., Shah, Z.: Optimization of response function on hydromagnetic buoyancy-driven rotating flow considering particle diameter and interfacial layer effects: homotopy and sensitivity analysis. Int. Commun. Heat Mass Transf. 144, 106770 (2023b)
- Díaz, F.F., Montes, J.B., Villamor, J.D., Fernández, S.Z.: Enhancing and Optimization in Exisiting HVAC Equipment Using Tools of Industry 4.0. J. Build. Eng., 111924 (2025)
- Farooq, U., Maatki, C., Kriaa, K., Hadrich, B., Imran, M., Noreen, S., Akgül, A., et al.: Characteristics of sodium alginate-based hybrid nanofluid and Darcy-Forchheimer flow induced by stretching surface with thermal radiation and Cattaneo-Christov heat flux model. J. Comput. Sci. 76, 102209 (2024)
- Hayat, T., Alsaedi, A., Razaq, A., Khan, S.A.: HARK formulation for entropy optimized convective flow beyond constant thermophysical properties. Case Stud. Therm. Eng. 54, 103983 (2024)
- Hussain, S., Rasheed, K., Ali, A., Vrinceanu, N., Alshehri, A., Shah, Z.: A sensitivity analysis of MHD nanofluid flow across an exponentially stretched surface with non-uniform heat flux by response surface methodology. Sci. Rep. 12(1), 18523 (2022)
- Hussanan, A., Aman, S., Ismail, Z., Salleh, M.Z., Widodo, B.: Unsteady natural convection of sodium alginate viscoplastic Casson based based nanofluid flow over a vertical plate with leading edge accretion/ablation. J. Adv. Res. Fluid Mech. Therm. Sci. 45, 92–98 (2018)
- Hussanan, A., Qasim, M., Chen, Z.M.: Heat transfer enhancement in sodium alginate based magnetic and non-magnetic nanoparticles mixture hybrid nanofluid. Phys. A, Stat. Mech. Appl. 550, 123957 (2020)
- Irfan, M., Khan, M., Khan, W.A.: Numerical analysis of unsteady 3D flow of Carreau nanofluid with variable thermal conductivity and heat source/sink. Results Phys. 7, 3315–3324 (2017)
- Jamshed, W., Goodarzi, M., Prakash, M., Nisar, K.S., Zakarya, M., Abdel-Aty, A.H.: Evaluating the unsteady Casson nanofluid over a stretching sheet with solar thermal radiation: an optimal case study. Case Stud. Therm. Eng. 26, 101160 (2021)
- Jegan, J., Suresh, R., Subramanian, E.K., Ramachandran, A., Reddy, S.R.R., Jakeer, S.: Analysis of numerical computation and ANN modelling on the bio-magnetic Darcy-Forchheimer ternary hybrid nanofluid flow: entropy generation. BioNanoScience 14(3), 2602–2624 (2024)
- Jubair, S., Ali, B., Kumar, A., Ahmad Ansari, M.: Numerical simulation of nonlinear flow and energy dynamics through spinning flow of Casson hybrid nanofluid past an extending surface. Part. Sci. Technol., 1–13 (2025)



- Khan, A., Khan, D., Khan, I., Ali, F., Imran, M.: MHD flow of sodium alginate-based Casson type nanofluid passing through a porous medium with Newtonian heating. Sci. Rep. 8(1), 1–12 (2018)
- Khan, A., Khan, D., Khan, I., Taj, M., Ullah, I., Aldawsari, A.M., Sooppy Nisar, K., et al.: MHD flow and heat transfer in sodium alginate fluid with thermal radiation and porosity effects: fractional model of Atangana–Baleanu derivative of non-local and non-singular kernel. Symmetry 11(10), 1295 (2019)
- Kierzenka, J., Shampine, L.F.: A BVP solver that controls residual and error. J. Numer. Anal. Ind. Appl. Math. 3(1-2), 27–41 (2008)
- Kumar, R.N., Gowda, R.P., Alam, M.M., Ahmad, I., Mahrous, Y.M., Gorji, M.R., Prasannakumara, B.C.: Inspection of convective heat transfer and KKL correlation for simulation of nanofluid flow over a curved stretching sheet. Int. Commun. Heat Mass Transf. 126, 105445 (2021)
- Kumar, M.D., Gurram, D., Yook, S.J., Raju, C.S.K., Shah, N.A.: Optimizing Thermal Performance of Water-Based Hybrid Nanofluids with Magnetic and Radiative Effects over a Spinning Disc. Chemom. Intell. Lab. Syst., 105336 (2025)
- Lund, L.A., Asghar, A., Rasool, G., Yashkun, U.: Magnetized Casson SA-hybrid nanofluid flow over a permeable moving surface with thermal radiation and Joule heating effect. Case Stud. Therm. Eng. 50, 103510 (2023)
- Moltot, A.T., Gorfie, E.H., Zergaw, G.A., Assres, H.D.: Influences of Cattaneo-Christov heat-mass fluxes and viscous dissipation on stagnation point Casson hybrid nanofluid flow over a stretching sheet with nonlinear thermal radiation. J. Appl. Math. 2025(1), 8837740 (2025)
- Nadeem, S., Ishtiaq, B., Ben Hamida, M.B., Almutairi, S., Ghazwani, H.A., Eldin, S.M., Al-Shafay, A.S.: Reynolds nano fluid model for Casson fluid flow conveying exponential nanoparticles through a slandering sheet. Sci. Rep. 13(1), 1953 (2023)
- Priyadharshini, P., Vanitha Archana, M.: Dynamics of magnetized hybrid solid particles in a rotating cone with gradient descent optimization. Numer. Heat Transf., Part B, Fundam., 1–20 (2024)
- Priyadharshini, P., Karpagam, V., Shah, N.A., Alshehri, M.H.: Bio-convection effects of MHD Williamson fluid flow over a symmetrically stretching sheet: machine learning. Symmetry 15(9), 1684 (2023)
- Raptis, A., Perdikis, C., Takhar, H.S.: Effect of thermal radiation on MHD flow. Appl. Math. Comput. 153(3), 645–649 (2004)
- Raza, J., Mebarek-Oudina, F., Ali, H., Sarris, I.E.: Slip effects on Casson nanofluid over a stretching sheet with activation energy: RSM analysis. Front. Heat Mass Transf. 22(4), 1017–1041 (2024)
- Razaq, A., Hayat, T., Khan, S.A., Momani, S.: ATSS model based upon applications of Cattaneo-Christov thermal analysis for entropy optimized ternary nanomaterial flow with homogeneous-heterogeneous chemical reactions. Alex. Eng. J. 79, 390–401 (2023)
- Rehman, A., Khan, D., Mahariq, I., Elkotb, M.A., Elnaqueb, T.: Viscous dissipation effects on time-dependent MHD Casson nanofluid over stretching surface: a hybrid nanofluid study. J. Mol. Liq. 408, 125370 (2024)
- Sajjan, K., Ahammad, N.A., Raju, C.S.K., Prasad, M.K., Shah, N.A., Botmart, T.: Study of nonlinear thermal convection of ternary nanofluid within Darcy-Brinkman porous structure with time dependent heat source/sink. AIMS Math. 8(2), 4237–4260 (2023)
- Samal, S., Mushahary, P., Ontela, S.: Heat transfer sensitivity and entropy analysis in electroosmotic-Casson radiative hybrid nanofluid squeezing flow with bioconvection. J. Therm. Anal. Calorim., 1–30 (2025)
- Shah, Z., Asghar, A., Ying, T.Y., Lund, L.A., Alshehri, A., Vrinceanu, N.: Numerical investigation of sodium alginate-alumina/copper radiative hybrid nanofluid flow over a power law stretching/shrinking sheet with suction effect: a study of dual solutions. Results Eng. 21, 101881 (2024)
- Shahzad, F., Jamshed, W., Nisar, K.S., Nasir, N.A.A.M., Safdar, R., Abdel-Aty, A.H., Yahia, I.S.: Thermal analysis for Al₂O₃-sodium alginate magnetized Jeffrey's nanofluid flow past a stretching sheet embedded in a porous medium. Sci. Rep. 12(1), 3287 (2022)
- Shankaralingappa, B.M., Madhukesh, J.K., Sarris, I.E., Gireesha, B.J., Prasannakumara, B.C.: Influence of thermophoretic particle deposition on the 3D flow of sodium alginate-based Casson nanofluid over a stretching sheet. Micromachines 12(12), 1474 (2021)
- Sharma, B., Kumar, S., Paswan, M.K.: Numerical investigation of MHD stagnation-point flow and heat transfer of sodium alginate non-Newtonian nanofluid. Nonlinear Eng. 8(1), 179–192 (2019)
- Thumma, T., Pyari, D.R., Ontela, S., Al-Mdallal, Q.M., Jarad, F.: Heat transfer analysis of magnetized Cu-Ag-H2O hybrid nanofluid radiative flow over a spinning disk when the exponential heat source and Hall current are substantial: optimization and sensitivity analysis. Case Stud. Therm. Eng. 50, 103448 (2023)
- Thumma, T., Al-Mdallal, Q.M., Dawar, A., Ontela, S., Reddy, N.K.: Homotopy and sensitivity analysis on hybrid nanofluid transient flow past a spinning sphere considering heat source and nonlinear thermal radiation: an optimization study. Alex. Eng. J. 117, 311–324 (2025)
- Yusuf, T.A.: Entropy analysis of unsteady MHD nanofluid flow over a stretching surface with effects of variable viscosity and nonuniform heat generation. Numer. Heat Transf., Part A, Appl. **85**(16), 2754–2771 (2024)



- Yusuf, T.A., Adeosun, A.T., Akinsola, V.O., Lebelo, R.S., Akinremi, O.J.: Numerical investigation for nonlinear thermal radiation in MHD Cu-water nanofluid flow in a channel with convective boundary conditions. Mathematics 11(15), 3409 (2023)
- Yusuf, T.A., Salawu, S.O., Adesanya, S.O., Ukaegbu, J.C.: Irreversibility analysis in an electro-osmotically driven flow using ternary hybrid nanofluids in a microchannel with a porous material. Z. Angew. Math. Mech. 104(12), e202300667 (2024)
- Zaki, A.M., Zayed, M.E., Bargal, M.H., Saif, A.G.H., Chen, H., Rehman, S., El-deen, E.S.H.N., et al.: Environmental and energy performance analyses of HVAC systems in office buildings using boosted ensembled regression trees: Machine learning strategy for energy saving of air conditioning and lighting facilities. Process Saf. Environ. Prot., 107214 (2025)
- Zeeshan, A., Hussain, D., Asghar, Z., Bhatti, M.M., Duraihem, F.Z.: Thermal optimization of MHD nanofluid over a wedge by using response surface methodology: sensitivity analysis. Propuls. Power Res. 12(4), 556-567 (2023)
- Zhang, K., Raju, C.S.K., Sajjan, K., Almutairi, B., Shah, N.A., Eldin, S.M.: Nonlinear free convective with longitudinal slits in the presence of super-hydrophobic and non-hydrophobic microchannels in a suspension of nanoparticles: multi-linear regression analysis. Case Stud. Therm. Eng. 49, 103138 (2023)
- Zohora, F.T., Akter, F., Haque, M.A., Chowdhury, N.M., Haque, M.R.: A novel pin finned structure-embedded microchannel heat sink: CFD-data driven MLP, MLR, and XGBR machine learning models for thermal and fluid flow prediction. Energy 307, 132646 (2024)

Publisher's note Springer Nature remains neutral with regard to jurisdictional claims in published maps and institutional affiliations.

Springer Nature or its licensor (e.g. a society or other partner) holds exclusive rights to this article under a publishing agreement with the author(s) or other rightsholder(s); author self-archiving of the accepted manuscript version of this article is solely governed by the terms of such publishing agreement and applicable law.

